Inorganic Chemistry

Article

pubs.acs.org/IC

Computational Insight into a Gold(I) N-Heterocyclic Carbene Mediated Alkyne Hydroamination Reaction

Madanakrishna Katari, Mitta Nageswar Rao, Gopalan Rajaraman,* and Prasenjit Ghosh*

Department of Chemistry Indian Institute of Technology Bombay, Powai, Mumbai 400 076, India

Supporting Information

ABSTRACT: A gold(I) N-heterocyclic carbene (NHC) complex mediated hydroamination of an alkyne has been modeled using density functional theory (DFT) study. In this regard, alkyne and amine coordination pathways have been investigated for the hydroamination reaction between two representative substrates, namely, MeC≡CH and $PhNH_2$, catalyzed by a gold(I) NHC based (NHC)AuCl-type pre-catalyst, namely, [1,3-dimethylimidazol-2-ylidene]gold chloride. The amine coordination pathway displayed a lower activation barrier than the alkyne coordination pathway. The catalytic cycle is proposed to proceed via a crucial proton-transfer step occurring between the intermediates $[(NHC)AuCH{=}CMeNH_2Ph]^+$ (**D**) and $[(NHC)Au(PhNHMeC{=}CH_2)]^+$ (**E**), the activation barrier of which was found to be significantly reduced by a proton relay mechanism process assisted by the presence of any adventitious H_2O molecule or even by any of the reacting $PhNH_2$ substrates. The final hydroaminated enamine product, $PhNHMeC{=}CH_2$, was further seen to be stabilized in its tautomeric imine form $PhN{=}CMe_2$.

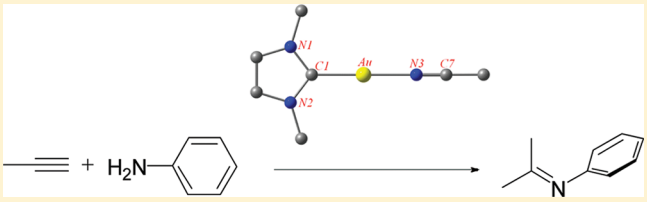

INTRODUCTION

Recently, the addition reactions, particularly of the H-heteroatom ones across unsaturated substrates, have generated renewed interest for providing direct atom economic access to many important P-, S-, N-, and O-containing compounds.[1] Additionally, because these addition reactions provide a greener alternative to the contemporary substitution reactions for yielding the same product, they have come in vogue in day-to-day organic synthesis. Quite interestingly though, while most of organometallic chemistry focuses on C−C or C−H addition, the counterpart examples of C- and H-heteroatom additions have received comparatively less attention, an observation that aroused our interest in the area. Hydroamination of olefins[2] and alkynes[3] is one such resourceful reaction that facilitates one-step 100% atom efficient conversion of cheap and readily available substrates to more valuable N-containing compounds of use as pharmaceuticals and agro, bulk, and fine chemicals.[4] Like the olefinic substrates, which provide direct access to higher substituted amines, the terminal alkynes lead to synthetically important compounds like aldimines and enamines, which are key intermediates to valuable target molecules in organic synthesis. Thus, rather than remaining confined as a mere aesthetic academic accomplishment, these reactions have gained greater relevance in the industrial world under the present day scenario. Of the two, however, hydroamination of alkynes is more facile owing to a rather weaker π bond in alkynes by ca. 70 kJ/mol than in olefins[5,6] and, hence, these reactions are relatively more well-understood than those of the alkenes, which largely remain restricted to activated olefins. Although condensation of carbonyl compounds and primary amines is an established method for the synthesis of imines, hydroamination of alkynes attracts interest as an environmentally friendly alternative,[7] and many new catalysts have been developed to perform these reactions.[3] It is to be noted here that the intermolecular version of this reaction involves aminomercuration of alkynes and requires a stoichiometric amount of mercury(II).[8] A number of metal catalysts, such as zinc, titanium, lanthanide, actinide, ruthenium, rhodium, and palladium, have been reported for this hydroamination reaction, but the yields and catalytic efficiencies for these catalysts are not yet satisfactory for practical explorations and thus the design and synthesis of new catalysts remain an intriguing challenge.[7] In this regard, also notable are the recent efforts in performing metal-free hydroamination reactions.[9] Thus, apart from the design and synthesis aspects, understanding the mechanism of such reactions is vital to the development of greener alternatives to the existing industrial standard methods.

Key challenges of hydroaminations, however, stem from the thermoneutrality and entropically unfavorable nature of these reactions arising out of their electron-rich reactant entities, i.e., the amines and alkynes or olefins, which are averse to mutual reaction.[4,5] It is worth noting that metals, depending upon their type, play a pivotal role in catalyzing these reactions under mild conditions by invoking different substrate activation pathways, namely, involving alkyne, alkene, or amine activations.[10] For example, the late transition metals, being carbophilic, often activate the olefins and alkynes by coordination to the metal center. A persistent issue frequently encountered in hydroaminations is in the regiochemistry of the products formed in

Received: November 15, 2011
Published: May 7, 2012

   dx.doi.org/10.1021/ic2024605 | Inorg. Chem. 2012, 51, 5593−5604

Scheme 1

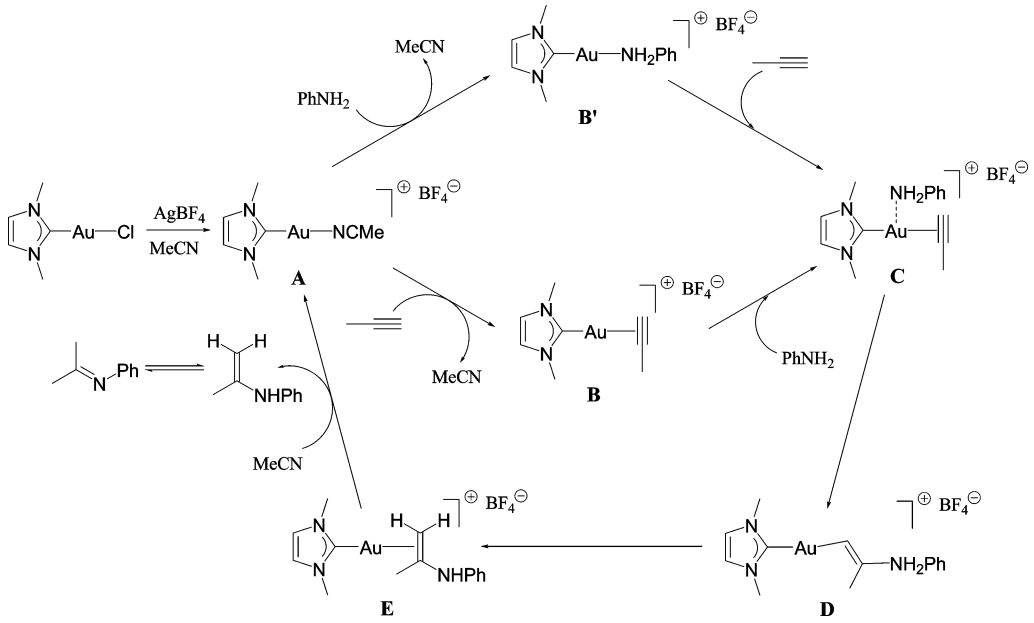

the case of asymmetrically substituted substrates. In this regard, we have recently observed regiospecific Markovnikov-type addition in hydroamination of arylamines with terminal alkynes by (NHC)AuCl-type precatalysts, namely, [1-R-4-R′-1,2,4-triazol-5-ylidene]AuCl [R = CH_2CO^tBu, CH_2CONH^tBu, and $C_6H_{10}OH$; R′ = CH_2Ph and CH_2CO^tBu].[11] With our 2-fold interest being in catalytic applications of N-heterocyclic carbene (NHC) based transition-metal complexes[12] in transformations of relevance to organic synthesis,[13−16] including that of hydroamination of alkenes[17] and terminal alkynes,[11] and also in the subsequent understanding of the catalyst mode of action from a mechanistic perspective,[18] we set out to obtain insight into hydroamination of terminal acetylenes by an (NHC)AuCl-type precatalyst with the aid of the density functional theory (DFT) study. It is worth noting that, despite the importance and surge in recent activities on these addition reactions, such studies remain surprisingly sparse in the literature to date,[19] even though the gold-catalyzed hydroamination reaction was investigated by Utimoto and co-workers as early as 1987.[20] Very recently, the mechanism of a gold(I)-mediated hydroamination of alkynes with ammonia was investigated using DFT methods, and the pivatol role of gold(I) in the catalytic cycle was established.[21] Unlike the hydroamination reaction, however, a detailed investigation on alkyne activation by gold using relativistic methods[22] along with its addition to alcohol and H_2O has been reported in considerable depth recently.[23]

Here in this contribution, we report the modeling of alkyne and amine coordination pathways for the hydroamination reaction of MeC≡CH and $PhNH_2$ as catalyzed by a gold(I) NHC precatalyst, namely, [1,3-dimethylimidazol-2-ylidene]gold chloride, with the aid of DFT studies (Schemes 1 and 2a,b). Additionally, molecular orbital (MO), natural bond orbital (NBO), and charge decomposition analysis (CDA) have been performed to understand the donor−acceptor nature of the species involved in the potential energy surface.

RESULTS AND DISCUSSION

A computational study was undertaken of a mechanistic cycle proposed based on our earlier observation of hydroaminations of terminal alkynes[11] with arylamines as catalyzed by a series of gold(I) (NHC)AuCl-type precatalysts, namely, [1-R-4-R′-1,2,4-triazol-5-ylidene]AuCl [R = CH_2CO^tBu, CH_2CONH^tBu, and $C_6H_{10}OH$; R′ = CH_2Ph and CH_2CO^tBu], in the presence of $AgBF_4$ at 90 °C and 12 h of reaction time. The hydroamination reaction was thus anticipated to initiate with a solvent-coordinated species, $[(NHC)Au(MeCN)]^+BF_4^-$, formed from the reaction of the (NHC)AuCl-type precatalyst with $AgBF_4$, on the basis of mass spectrometric evidence (Scheme 1). In the present study, appropriate ligand modifications, like the selection of simple methyl moieties as N-substituents as opposed to the more elaborate functional groups on the NHC ligands in our reported gold(I) hydroamination precatalysts,[11] and the assumption of the initiating species being an isolated cationic solvent-coordinated species, $[(NHC)Au(MeCN)]^+$ (**A**), in lieu of an ionic $[(NHC)Au(MeCN)]^+BF_4^-$ compound with a noncoordinating BF_4^- anion, were adopted for computational simplicity. It is worth noting that recent theoretical studies indicate that the C−N bond distances and C−N−C bond angles are related to the σ-donor and π-acceptor properties of the NHC ligands.[24] Because we found that only minor differences exist between the structural parameters of the methyl-substituted models and the more elaborate functional groups of the NHC ligands, we believe that current simplified model systems are appropriate for undertaking the proposed computational study. In particular, the hydroamination reaction was modeled for two representative substrates, MeC≡CH and $PhNH_2$, as catalyzed by a cationic species, $[(1,3\text{-dimethylimidazol-2-ylidene})Au(MeCN)]^+$ (**A**). The stationary and transition states of the proposed catalytic cycle were computed at the B3LYP/SDD, 6-31G(d) level of theory by applying suitable modification to the solid-state structure of the reported precatalysts,[11] whose coordinates were obtained from X-ray analysis (see Figures S1−S18 and S29−S36 and Tables S1−S25 in the Supporting Information). Further corroboration of the computational results was obtained by performing single-point calculations using higher a triple ξ-basis set at the B3LYP/SDD, TZVP level of theory. Because cationic species were assumed for modeling, solvent effects were incorporated via polarizable continuum model (PCM) calculations, the values of which are used in the current discussion.

dx.doi.org/10.1021/ic2024605 | Inorg. Chem. 2012, 51, 5593−5604

Scheme 2. Computed Catalytic Cycle for Hydroamination of MeC≡CH with $PhNH_2$ by a Solvent-Bound Initiating Species A Depicting Both the Amine and Alkyne Coordination Pathways Proceeding via a H_2O-Mediated Proton-Transfer Step (a) and a $PhNH_2$-Mediated Proton-Transfer Step (b)

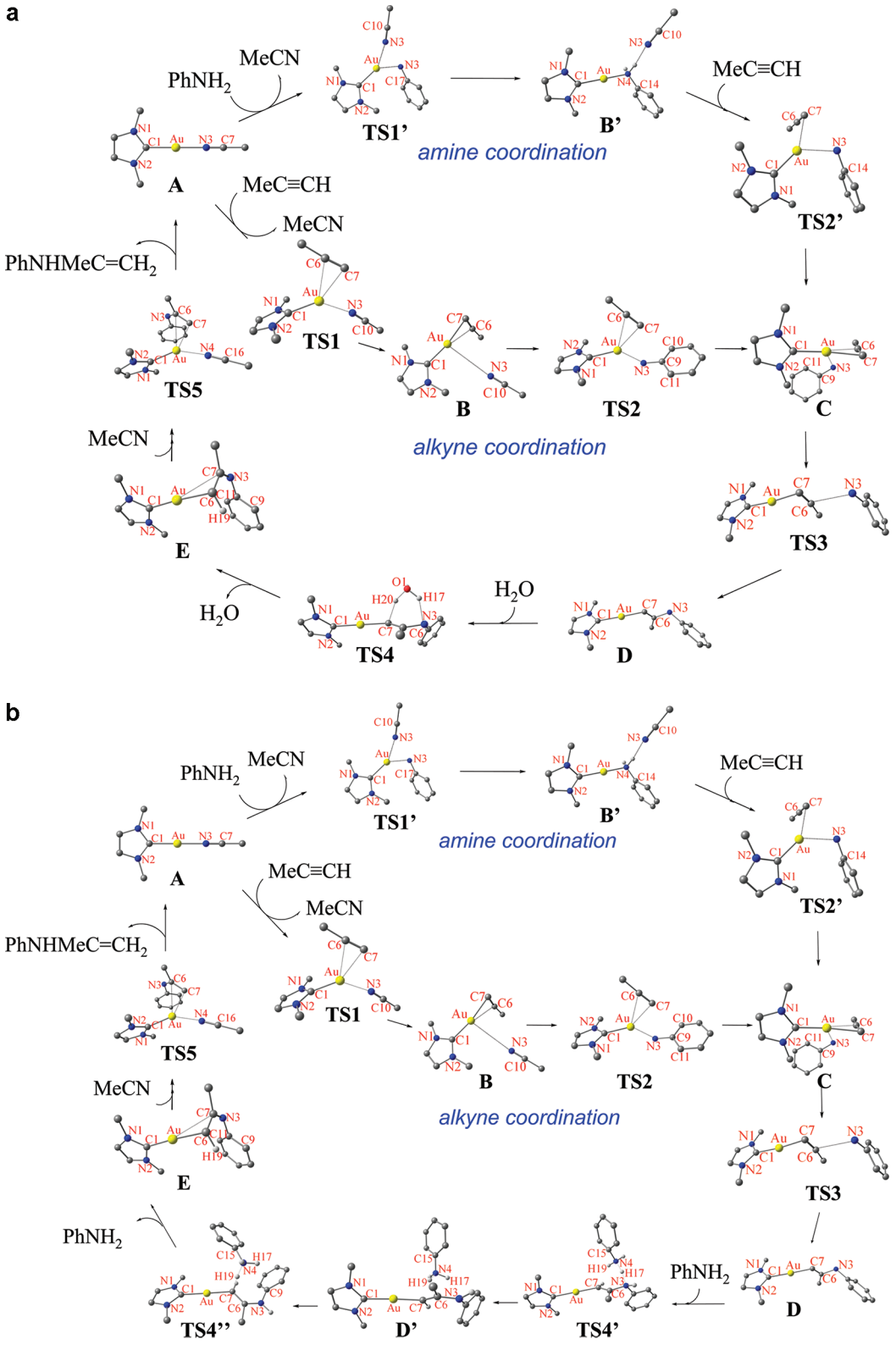

In particular, the alkyne and amine coordination pathways have been investigated for the hydroamination reaction. The free-energy profiles of the reaction trajectory in an isolated gaseous phase as well as in a solvent (MeCN) phase, specifically chosen in keeping with the experimental conditions, were eventually computed for obtaining a better understanding of the catalyst mode of action (Figure 3a,b, Scheme 2a,b, and Figures S24–S26 in the Supporting Information).

The metal–ligand donor–acceptor interaction of the type donor–[NHC]Au^I (acceptor) [donor = MeCN in **A**, MeC≡CH and

dx.doi.org/10.1021/ic2024605 | Inorg. Chem. 2012, 51, 5593–5604

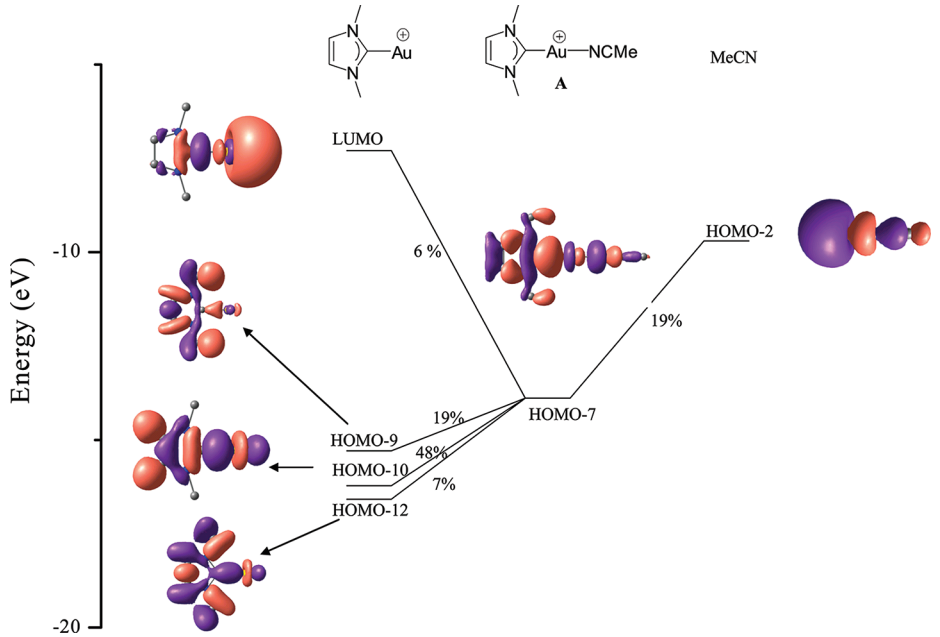

Figure 1. Simplified orbital interaction diagram showing the major contribution of the $[(NHC)Au{-}MeCN]^{+}$ bond in **A**.

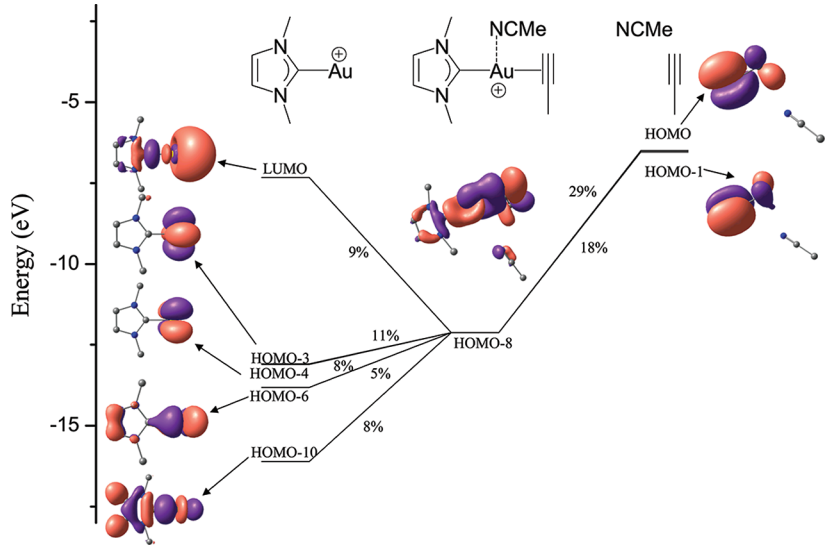

Figure 2. Simplified orbital interaction diagram showing the major contribution of the $[(NHC)Au(CH{\equiv}CMe)]^{+}{\cdot}MeCN$ bond in **B**.

MeCN in **B**, $PhNH_2$ and MeCN in **B′**, MeC≡CH and $PhNH_2$ in **C**, $PhNH_2MeC{\equiv}CH-$ in **D**, PhNHMeC═CH− and $PhNH_3$ in **D′**, and $PhNHMeC{=}CH_2$ in **E**] in the stationary points **A**−**E** were probed using CDA studies, and for deeper insight into these interactions, the corresponding MO correlation diagrams were constructed from the individual fragment molecular orbitals (FMOs) of the donor and $[NHC]Au^{I}$ (acceptor) fragments (see Figures 1 and 2 and Figures S19−S23 and Table S26 in the Supporting Information). The donor → $[NHC]Au^{I}$ (acceptor) σ interaction is represented by d, while the corresponding donor ← $[NHC]Au^{I}$ (acceptor) π interaction is represented by b, and a d/b ratio thus signifies the relative extent of forward σ donation to π back-donation occurring between the donor and acceptor fragments in the **A**−**E** intermediates.

Of particular interest is the initial originating species, which incidentally is a solvent-coordinated cationic species, **A**, as observed experimentally,[11] and is common to both the proposed alkyne and amine coordination pathways. Quite expectedly, the computed structure of the initiating species, **A** (see Figure S1 and Table S5 in the Supporting Information), showed a linear geometry (∠C1−Au−N3 = 179.9°) at the gold(I) center with the metal bound to carbene carbon atom and a solvent MeCN nitrogen atom at two of its sides, in concurrence with the common coordination observed for the d^{10} configuration of gold(I).[25] The Au−C1 (carbene carbon) bond length of 2.012 Å and the Au−N3 (acetonitrile nitrogen) bond length of 2.058 Å were in good agreement with the respective single-bond distances equivalent to the sum of the individual covalent radii of the bonding atoms (Au−C = 2.108 Å and Au−N = 2.036 Å).[26] Before we begin, it is important to describe the bonding in species **A** in detail to gain understanding on the electronic origin of the difference in reactivity observed during the catalytic cycle. As previously has

dx.doi.org/10.1021/ic2024605 | *Inorg. Chem.* 2012, 51, 5593−5604

been described,[27] the bonding in (NHC)AuC1-type complexes, in general, can be viewed as a 3-center 4-electron σ bond, where the ligand and carbene donate electrons to the empty 6s orbital of the gold to form a strong σ bond. Owing to the presence of the second σ-donor ligand, trans to NHC, the bond order for Au−C1 reduces significantly. Additionally, the metal center is able to form two π bonds by donation from perpendicular filled d orbitals to the empty π acceptor on the ligand and NHC[27] (see Figures S1 and S2 in the Supporting Information). These two bonds compete for electron density from gold, and thus back-donation to carbon is thus affected, leading to an alteration in the Au−C1 bond order. The Au−C1 distance in the $[(NHC)Au]^+$ species is found to be 1.99 Å, revealing a rather weak trans influence of MeCN on the Au−C1 π back-donation in **A**. Besides, NBO analysis indicates that the Au−C1 σ bond is significantly ionic in character with donation of 80% from the carbon atom and 20% from the gold atom for **A**. On the other hand, the Au−N σ bond is found to be much more ionic because here the gold contribution accounts for less than 10%. Quite expectedly, consistent with the weak π-acidic nature of the MeCN fragment, the $[NHC]Au^I$ (acceptor)−(MeCN) (donor) bond was indeed found to be predominantly a σ-type interaction, as observed from a high d/b ratio (19) in CDA analysis (see Table S26 in the Supporting Information). The $[NHC]Au^I$−(MeCN) bond dissociation energy (D_e) was estimated to be 28.6 kcal/mol in the solvent (MeCN) phase at the B3LYP/SDD, TZVP level of theory (see Table S27 in the Supporting Information). More specifically, the MO corresponding to the $[NHC]Au^I$−(MeCN) σ interaction exhibited σ donation from the nitrogen lone pair of MeCN to a metal-based d-type FMO of the $[NHC]Au^I$ fragment of the initiating species **A** (see Figure 1). The solvent-coordinated species **A** may then proceed along an alkyne or an amine coordination pathway, as discussed below (see Schemes 1 and 2a,b).

Alkyne Coordination Pathway. The alkyne coordination catalytic cycle initiates with a cationic solvent-coordinated species, **A**, undergoing an alkyne coordination step that exhibits an energy barrier of 17.4 kcal/mol (solvent phase), yielding a cationic acetylene-coordinated species, $[(NHC)Au(MeC{\equiv}CH)]^+{\cdot}MeCN$ (**B**), with elimination of a MeCN molecule. The transition state TS1 undergoes dissociation of the Au−MeCN bond, exhibiting an elongated Au···N3 (acetonitrile nitrogen) distance (2.335 Å) compared to that in the starting reactant species **A** (2.058 Å), followed by an alkyne coordination of MeC≡CH in the form of a weak interaction arising out of relatively long Au···C6 (alkyne carbon, 2.653 Å) and Au···C7 (alkyne carbon, 2.523 Å) distances (see Figure S3 and Table S6 in the Supporting Information). The computed imaginary frequency (i96 cm^{-1}) is consistent with the picture described above. The optimized structure of TS1, thus, confirms the solvent dissociation and alkyne association events happening synchronously in the transition state TS1. The approach of π-acidic alkyne to gold in TS1 leads to a decrease in back-donation for the Au−C1 bond, resulting in elongation of the Au−C1 bond by 0.027 Å in TS1. The transition state TS1 results in an alkyne-coordinated intermediate **B** (see Figure S5 and Table S8 in the Supporting Information), which showed a near-linear geometry (∠C1−Au−C7 = 166.3°) at the metal. This species was slightly endothermic from the corresponding reactant (6.0 kcal/mol). The methyl acetylene molecule was strongly bound to the metal in the alkyne-bound intermediate **B**, as was evident from the observed shorter Au−C (alkyne carbon) bond distances [d(Au−C6) = 2.346 Å and d(Au−C7) = 2.215 Å] in comparison to the corresponding ones [d(Au···C6) = 2.653 Å and d(Au···C7) = 2.523 Å] observed earlier in the preceding transition state TS1. Quite interestingly though, in contrast to the $[NHC]Au^I$ (acceptor)−(MeCN) (donor) σ-type interaction in **A** that exhibited a high d/b ratio of 19, the $[NHC]Au^I$ (acceptor)−(MeC≡CH and MeCN) (donor) interaction in **B** had significantly more π-back-bonding character, as reflected in a low d/b ratio of 5.91, in concurrence with the π-acidic nature of an alkyne ligand (see Figure 2 and Table S26 in the Supporting Information). The $[NHC]Au^I$−(MeC≡CH) D_e was estimated to be 27.6 kcal/mol in the solvent (MeCN) phase at the B3LYP/SDD, TZVP level of theory considering negligible contribution from the weakly bound MeCN moiety to the metal (see Table S27 in the Supporting Information). The MO correlation diagram showed that the $[NHC]Au^I$ (acceptor)−(MeC≡CH and MeCN) (donor) bond in **B** is composed of an interaction between a π-type FMO of the MeC≡CH moiety and a d-type FMO of the $[NHC]Au^I$ fragment (Figure 2).

The alkyne-coordinated intermediate **B** subsequently reacts with aniline via transition state TS2, giving an amine- and an alkyne-bound cationic intermediate species $[(NHC)Au(MeC{\equiv}CH)(PhNH_2)]^+$ (**C**). Although there exists a possible pathway where the amine can directly approach the coordinated alkyne to form the species **D**, a recent experimental study indicates that N−C coupling occurred via a coordinated gold−amine type species,[28] which led us to route the mechanism via TS2 to reach the species **D**. The transition state TS2 exhibited an activation barrier of 7.8 kcal/mol (solvent phase) from its nearest reactant species **B** and is characterized by an imaginary frequency of i82 cm^{-1} along the displacement vector in the direction of bond formation between the gold and N3 atoms of the $PhNH_2$ moiety. Quite interestingly, the formation of **C** is marginally exothermic with respect to **B**, with the net energy indicating that it is a rather thermonetural speices (−0.3 kcal/mol). The observed Au−C (alkyne carbon) distances [d(Au···C6) = 2.755 Å and d(Au···C7) = 2.479 Å] and the Au−N3 (aniline nitrogen) distance [d(Au···N3) = 2.408 Å] in the transition state TS2 are suggestive of the presence of weak interactions between the gold center to the methyl acetylene and the aniline molecules (see Figure S7 and Table S10 in the Supporting Information). The Au−C1 distance in TS2 is further elongated compared to TS1 and **B**, indicating the strong trans influence of amine compared to MeCN. The amine essentially decreases back-donation for the Au−C1 bond, resulting in elongation of the Au−C1 bond to 2.050 Å in TS2. The transition state TS2 connects to an amine- and an alkyne-bound cationic intermediate species **C** containing slightly more strongly bound alkyne [d(Au···C6) = 2.351 Å and d(Au−C7) = 2.210 Å] and a weakly bound amine [d(Au···N3) = 4.988 Å] moieties (see Figure S9 and Table S12 in the Supporting Information). Indeed, the MO correlation diagram showed that the $[NHC]Au^I$ (acceptor)−(MeC≡CH and $PhNH_2$) (donor) interaction was comprised of contributions from the FMOs of mainly the MeC≡CH moiety and a metal-based d type of the $[NHC]Au^I$ fragment (see Figure S20 in the Supporting Information). Neglecting the presence of a weak $[NHC]Au^I$ (acceptor)−($PhNH_2$) (donor) interaction, the $[NHC]Au^I$−(MeC≡CH) D_e was computed to be 27.8 kcal/mol in the solvent (MeCN) phase at the B3LYP/SDD, TZVP level of theory (see Table S27 in the Supporting Information). Like in **B**, the $[NHC]Au^I$ (acceptor)−(MeC≡CH and $PhNH_2$) (donor) interaction in **C** also exhibits significant π-back-bonding character, as displayed in

dx.doi.org/10.1021/ic2024605 | Inorg. Chem. 2012, 51, 5593−5604

a low d/b ratio of 5.89 (see Table S26 in the Supporting Information). Quite interestingly, the ∠C1−Au−C7 angle (166.0°) that the MeC≡CH moiety makes with the [NHC]Au^{I} fragment in **C** is identical with the one that it makes with the same fragment in **B**. The weakly bound $PhNH_2$ moiety makes an obtuse angle (∠C1−Au−N3 = 107.4°) with the [NHC]Au^{I} fragment in **C**. It is worth mentioning that, beyond the intermediate **C**, a common mechanistic pathway is proposed for both of the amine and alkyne coordination routes.

Amine Coordination Pathway. Analogous to the alkyne coordination, the amine coordination too initiates with coordination of an amine, $PhNH_2$, to the metal center of the solvent-coordinated initiating species **A** to yield an amine-coordinated intermediate $[(NHC)Au(PhNH_2)]^{+}\cdot MeCN$ (**B′**). Amine coordination exhibits an energy barrier of 10.4 kcal/mol at its transition state TS1′, which showed a slightly elongated Au···N3 (acetonitrile nitrogen) distance (2.346 Å) in comparison to that in the originating species **A** (2.058 Å). Similarly, a relatively long Au···N4 (amine nitrogen) distance (2.486 Å) of the metal-coordinated aniline was observed in the transition state TS1′ (see Figure S4 and Table S7 in the Supporting Information). The computed frequency (i77 cm^{-1}) corresponds to the displacement vectors in the direction of bond formation between gold and N4 atoms of the $PhNH_2$ moiety and the bond dissociation between the gold and N3 atoms in the MeCN moiety.

At this juncture, important is the comparison of the TS1 and TS1′ structures. Despite the structural differences that exist due to the approaching ligand (alkyne versus amine), the coordinating MeCN distances are merely equal in both transition states. On the contrary, the Au−C1 distance in TS1′ is found to be 2.015 Å compared to 2.039 Å in TS1, thereby clearly indicating that the decrease in the Au−C1 bond order due to amine coordination is much smaller than the coordination from an π-acidic alkyne ligand. This difference in the bond strengths makes TS1′ more stable by 7.0 kcal/mol compared to TS1.

The amine-coordinated intermediate **B′** showed a linear geometry at the metal center exhibiting a ∠C1−Au−N4 angle of 179.8°. The intermediate **B′** was slightly exothermic by −5.08 kcal/mol from the nearest reacting species **A**. As can be ascertained from a shorter Au−N (amine nitrogen) bond distance [d(Au−N4) = 2.139 Å] in **B′** with respect to the corresponding one observed in transition state TS1′ [d(Au···N4) = 2.486 Å], the aniline moiety was found to be tightly coordinated to the metal center (see Figure S6 and Table S9 in the Supporting Information). The coordinated amine−metal Au^{I}−($PhNH_2$) interaction, {[NHC]Au^{I} (acceptor)−($PhNH_2$ and MeCN) (donor)}, was purely σ-type, as observed from the CDA studies that showed a very high d/b ratio of 123, thereby implying the absence of any π back-donation (see Figure S19 and Table S26 in the Supporting Information). Compared to species **B**, where the π-acidic nature of alkyne leads to decrease in back-donation, thus resulting in a longer Au−C1 (2.037 Å) bond, species **B′** exhibits a relatively shorter Au−C1 bond (2.020 Å), indicative of a stronger Au−C1 back-donation in **B′**. The [NHC]Au^{I}−($PhNH_2$) D_e was calculated to be 35.7 kcal/mol in the solvent (MeCN) phase at the B3LYP/SDD, TZVP level of theory by considering a negligible contribution from the weakly bound MeCN moiety (see Table S27 in the Supporting Information). The MO correlation diagram showed that the [NHC]Au^{I} (acceptor)−($PhNH_2$ and MeCN) (donor) bond in **B′** is composed of an interaction between a σ-type FMO of the $PhNH_2$ moiety and a d-type FMO of the [NHC]Au^{I} fragment.

The amine-coordinated intermediate **B′** then reacts with MeC≡CH, yielding a very high-energy transition state TS2′ that displayed an activation barrier of 19.2 kcal/mol from its nearest reactant species **B′**. The alkyne coordination is less favorable because of a comparatively higher activation barrier by 8.8 kcal/mol from the preceding amine coordination step. The transition state TS2′ has been characterized by an imaginary frequency of i79 cm^{-1}, which exhibited a displacement vector in the direction of bond formation between the gold atom and C6 and C7 atoms of the MeC≡CH moiety. The transition state TS2′ showed slightly elongated Au−C (alkyne carbon) [d(Au···C6) = 2.751 Å and d(Au···C7) = 2.483 Å] and Au−N3 (aniline nitrogen) [d(Au···N3) = 2.516 Å] distances consistent with a weak interaction prevailing between the gold center and the MeC≡CH and $PhNH_2$ moieties (see Figure S8 and Table S11 in the Supporting Information). The presence of alkyne leads to a considerable increase in the Au−C1 distance, as seen from a Au−C1 distance of 2.020 Å in **B′** to that of 2.036 Å in TS2′. The transition state TS2′ led to an amine- and alkyne-coordinated species **C**, the formation of which was found to be endothermic with respect to **B′** by 10.7 kcal/mol. The intermediate **C** then follows a common route for the hydroamination reaction from beyond this point.

The amine- and alkyne-bound cationic intermediate species **C** undergoes Markovnikov addition by a nucleophilic attack of the coordinated amine nitrogen at the alkyne carbon, resulting in C−N bond formation, which subsequently also leads to Au−C bond formation, via a transition state TS3 that display an activation barrier of 4.9 kcal/mol (solvent phase) from the nearest reactant species **C**. It is worth noting that the regiochemistry of the hydroamination reaction is determined at this step, with the Markovnikov fashion of the addition being more favorable than the anti-Markovnokov addition (see Figures S28 and S33−S36 and Tables S22−S25 in the Supporting Information). The NBO-computed natural charges on the two carbon atoms (C6 and C7; see Figure S9 in the Supporting Information) are significantly different, with the value of +0.066 for the carbon attached to gold and −0.339 for the adjacent carbon, and this difference basically facilitates formation of the Markovnikov product. The transition state TS3 has been characterized by an imaginary frequency of i89 cm^{-1}, exhibiting displacement vectors in the direction of bond formation between C6 of the HC≡CMe moiety and N3 of the $PhNH_2$ moiety. The observed Au−C (alkyne carbon) distances [d(Au···C7) = 2.143 Å and d(Au···C6) = 2.675 Å] and (alkyne) C6−N3 (aniline) distance [d(C6···N3) = 2.705 Å] in the transition state TS3 are testimony to the amine N3 attack on the alkyne carbon atom toward the formation of a C−N bond (see Figure S10 and Table S13 in the Supporting Information). The transition state TS3 leads to the formation of a cationic intermediate species $[(NHC)AuCH{=}CMeNH_2Ph]^{+}$ (**D**), which exhibits a single-bond Au−C7 distance of 2.053 Å and a slightly elongated single-bond C6−N3 distance of 1.533 Å (see Figure S11 and Table S14 in the Supporting Information). The formation of species **D** is thus found to be energetically favorable by −14.0 kcal/mol with respect to the nearest reacting species **C**. This large stabilization compared to the other intermediates is due to the presence of strong σ donation occurring from the alkyne moiety to the gold(I) center, where 81% of the contribution for this σ bond is from the alkyne counterpart, as revealed by NBO analysis. The Au^{I}−($CH{=}CMeNH_2Ph$) σ interaction exhibited a very high D_e of 74.2 kcal/mol in the solvent (MeCN) phase at the

dx.doi.org/10.1021/ic2024605 | Inorg. Chem. 2012, 51, 5593−5604

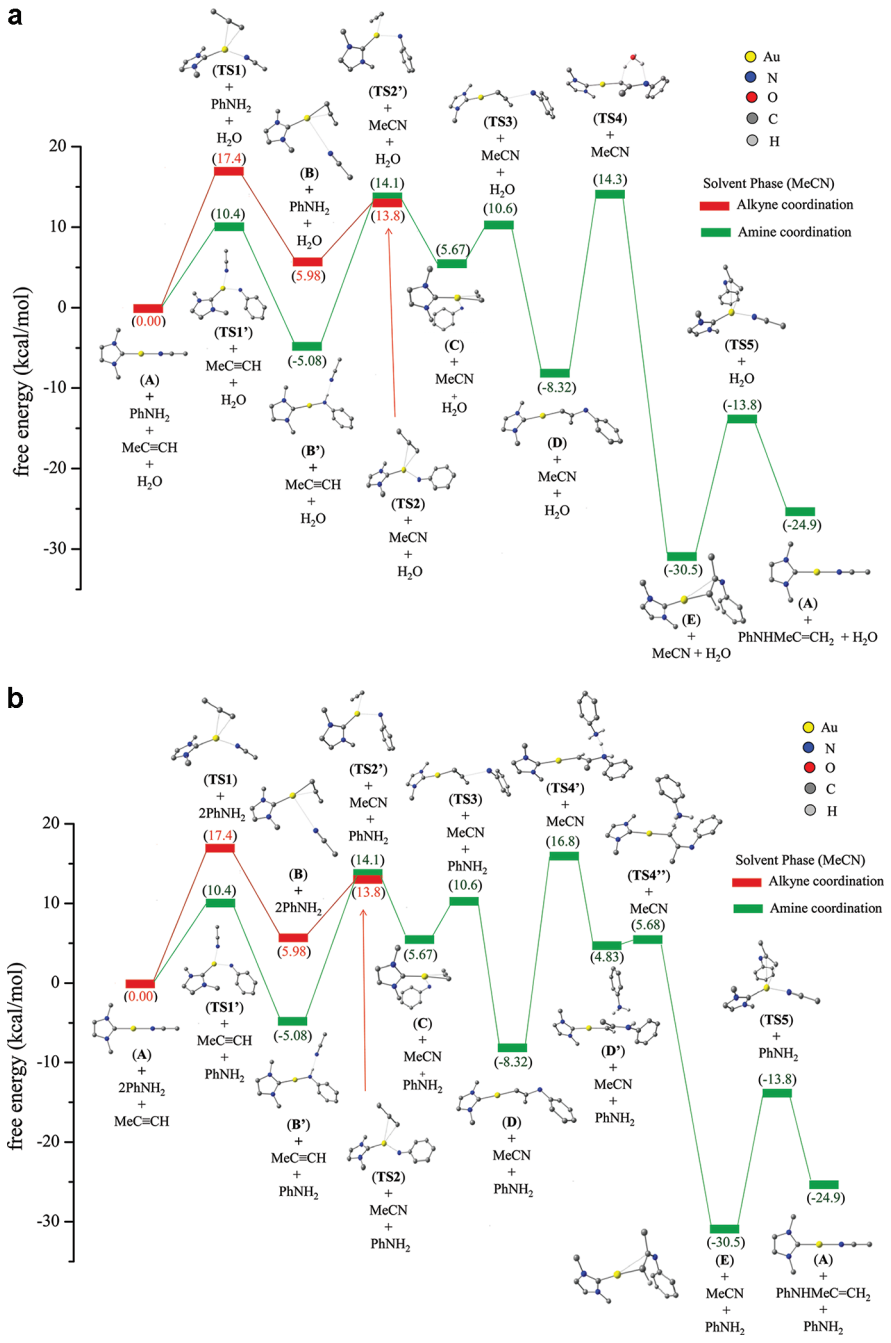

Figure 3. Overlay of the computed solvent (MeCN) phase free energies (ΔG) at the B3LYP/SDD, TZVP level of theory depicting amine and alkyne coordination pathways proceeding via a H_2O-mediated proton-transfer step (**a**) and a $PhNH_2$-mediated proton-transfer step (**b**) for hydroamination of MeC≡CH with $PhNH_2$ by a gold(I) precatalyst, [1,3-dimethylimidazol-2-ylidene]gold chloride, in the presence of $AgBF_4$ in MeCN: $\{(NHC)Au(MeCN)\}^+$ (**A**), $\{(NHC)Au(MeC{\equiv}CH)\}^+{\cdot}MeCN$ (**B**), $\{(NHC)Au(PhNH_2)\}^+{\cdot}MeCN$ (**B'**), $\{(NHC)Au(MeC{\equiv}CH)(PhNH_2)\}^+$ (**C**), $\{(NHC)AuCH{=}CMeNH_2Ph\}^+$ (**D**), and $\{(NHC)Au(PhNHMeC{=}CH_2)\}^+$ (**E**).

B3LYP/SDD, TZVP level of theory (see Table S27 in the Supporting Information). CDA analysis showed that the interaction is primarily of the σ type, as observed from a high d/b ratio of 12.4 (see Figure S18 and Table S26 in the Supporting Information). The ∠C1−Au−C7 angle was found to be 178.3°, while the ∠C7−C6−N3 angle was 117.5° in the intermediate species **D**. The Au−C1 bond is found to be further elongated to 2.072 Å, indicating a stronger trans σ donation and leading to a weakening of the Au−C1 bond.

The cationic intermediate species **D** undergoes a proton transfer between an amine N3 to an alkyne carbon (C7) assisted by a proton relay mechanism involving the possibility of the presence of any adventitious H_2O molecule or by any reacting $PhNH_2$ molecule, the prospects of which are discussed below (Scheme 2a,b and Figures 3a,b and 4).

H_2O-Mediated Proton Relay. The H_2O-assisted proton relay displays an activation barrier of 22.6 kcal/mol (solvent phase) with respect to the nearest reactant species **D** at a six-membered transition state TS4. Although the absolute barrier height computed seems to be high, the large barrier is primarily due to the large gain in the stabilization of species **C**. The net energy penalty due to the transition state is, in fact, found to be

dx.doi.org/10.1021/ic2024605 | Inorg. Chem. 2012, 51, 5593−5604

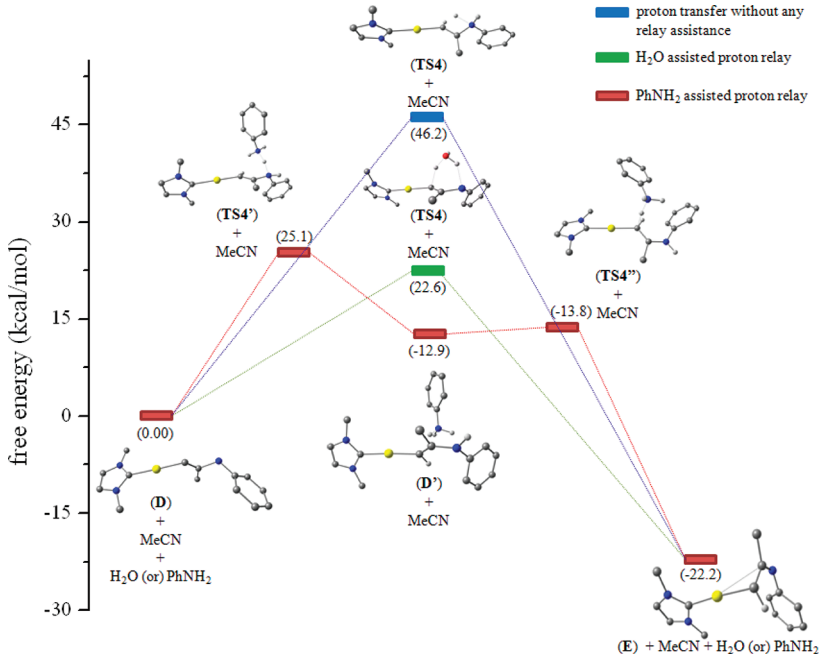

Figure 4. Overlay of the computed solvent (MeCN) phase free energies (ΔG) at the B3LYP/SDD, TZVP level of theory depicting a proton shuttle step (**D**→**E**) with H_2O (green) and $PhNH_2$ (red) and without any relay assistance (blue).

only 14.3 kcal/mol from species **A** (Scheme 2 and Figure 3). A large thermodynamic stability of **D** followed by a relatively higher barrier for protonation is perhaps the reason for the elevated temperature conditions required for the experimental setup to carry out the catalytic transformations.[11] The transition state TS4 was verified by the characteristic imaginary frequency of i571 cm^{-1} depicting a displacement vector in the direction of hydrogen atom transfer from N3 to C7 atoms via a H_2O molecule (see Figure S13 and Table S15 in the Supporting Information). Significantly enough, the role of the adventitious H_2O molecule in lowering the activation barrier of the reaction becomes very much evident from the fact that the corresponding proton transfer between the amine N3 and alkyne C7, without the H_2O molecule, displays a very high activation barrier of 46.2 kcal/mol (solvent phase) from species **D** at the B3LYP/SDD, TZVP of theory, which, consequently, would have made the proton-transfer step the rate-determining step of the whole reaction if an alternate low-energy pathway had not been explored (see Figures S12 and S24 and Table S16 in the Supporting Information). Because the computed (gas-phase) barrier is prohibitively high and because, experimentally, the reactions were conducted under aerobic conditions, the transition-state computation with an explicit H_2O molecule was thus rationalized. This was done primarily in view of the fact that significant reductions in the barrier heights were observed for the transition-state models having explicit solvent treatments and which thus underscores the importance of explicit solvation in understanding the mechanism of such reactions.[29] It is worth noting that, despite performing several experimental runs of the hydroamination reaction under varying amounts of H_2O as well as in its absence for the following representative substrates, PhC≡CH and 2,6-diethylaniline, by a representative precatalyst [1-(*N*-*tert*-butylacetamido)-4-benzyl-1,2,4-triazol-5-ylidene]gold chloride, we are unable to prove or refute the influence of H_2O in lowering the activation barrier of the proposed catalytic cycle for reasons that it is extremely difficult to rule out the presence of a minute amount of H_2O even under vigorously dry conditions given the fact that the H_2O molecule is required only in a catalytic amount and the presence of a single molecule is sufficient enough to carry out the whole conversion (see Figure S27 in the Supporting Information).

$PhNH_2$-Mediated Proton Relay. Apart from H_2O, we have also explored other possible proton shuttle agents, in particular aniline. The $PhNH_2$-assisted proton relay between the intermediates **D** and $[(NHC)Au(PhNHMeC{=}CH_2)]^+$ (**E**) is proposed to proceed in a two-step fashion because of the more bulky $PhNH_2$ compared to H_2O that assists the proton relay in a single-step sequence (Scheme 2a,b and Figure 3a,b). Thus, the first step of the $PhNH_2$-assisted relay involves proton transfer from an amine N3 in the intermediate **D** to $PhNH_2$, yielding transition state TS4′, which displays an activation barrier of 25.1 kcal/mol with respect to the nearest reactant species **D**. It is worth noting that the transition state TS4′ could only be characterized by freezing the phenyl ring (i.e., atoms C7, C15, C16, C17, C18, C19 C20, and N3) of the aniline moiety in the proximity of the metal center of the nearest reacting species **D**, and thus the activation barrier observed for TS4′ represents an upper limit of the energy barrier for the $PhNH_2$-assisted proton relay process. The transition state TS4′ was verified by a characteristic imaginary frequency of i434 cm^{-1}, which depicts a displacement vector in the direction of hydrogen atom transfer from N3 to N4 atoms of $PhNH_2$ (see Figure S14 and Table S17 in the Supporting Information). The transition state TS4′ yields an anilinium ion $[(PhNH_3)^+]$ bound cationic intermediate species $[(NHC)AuCH{=}CMeNHPh]\cdot(PhNH_3)^+$ (**D′**), which was endothermic by 4.83 kcal/mol with respect to initiating species **A**. Analogous to the linearity at the metal center observed in the intermediate species **A**–**D**, an angle ∠C1–Au–C7 of 177.5° was observed at the metal center in **D′** (see Figure S15 and Table S18 in the Supporting Information).

The intermediate species **D′** subsequently undergoes another intermolecular proton transfer from anilinium N4 to alkyne carbon (C7) to form an enamine-bound cationic intermediate

dx.doi.org/10.1021/ic2024605 | *Inorg. Chem.* 2012, 51, 5593–5604

species **E** via transition state TS4″. As expected, the transition state TS4″ exhibited an imaginary frequency of i268 cm^{-1} along displacement vectors in the direction of hydrogen atom transfer from N4 to C7 atoms of $PhNH_2$ (see Figure S16 and Table S19 in the Supporting Information) and exhibited an activation barrier of 5.68 kcal/mol with respect to the initial reacting species **A**. Overall, a significant reduction of the activation barrier for proton transfer between amine N3 and alkyne carbon (C7) was observed in the case of the H_2O- or $PhNH_2$-assisted proton relay processes (Figure 4).

Ultimately, both transition states TS4, in the case of the H_2O-assisted proton relay (Scheme 2a and Figure 3a), and TS4″, in the case of the $PhNH_2$-assisted proton relay (Scheme 2b and Figure 3b), converge to an enamine-bound cationic intermediate species **E**, which showed an unsymmetrically bound enamine [d(Au−C7) = 2.168 Å and d(Au···C6) = 2.878 Å] moiety to the gold center. The formation of this species is also thermodymically favorable by −30.5 kcal/mol with respect to the initiating species **A**. Similar to the linearity at the metal center observed in the intermediate species **A**−**D**, an angle (∠C1−Au−C7) of 175.0° was observed at the metal center in **E** (see Figure S17 and Table S20 in the Supporting Information). The enamine moiety in **E**, which exhibited a [NHC]Au^I−(PhNHMeC═CH_2) D_e of 45.1 kcal/mol, was thus more tightly bound to the gold(I) center than the corresponding MeCN moiety in **A** (28.6 kcal/mol), MeC≡CH and MeCN moieties in **B** (27.6 kcal/mol), and the MeC≡CH moiety in **C** (27.8 kcal/mol) in the solvent (MeCN) phase at the B3LYP/SDD, TZVP level of theory (see Table S27 in the Supporting Information). The MO corresponding to the [NHC]Au^I(PhNHMeC═CH_2) σ-bonding interaction showed electron donation between the enamine PhNHMeC═CH_2 and the [NHC]Au^I fragments. Consistent with the electron-rich nature of the enamine moiety PhNHMeC═CH_2, very little π back-donation was seen in **E**, as observed in a high d/b ratio of 16.7 compared to that in **A** (19), **B** (5.91), **C** (5.89), and **D** (12.4) (see Figure S23 and Table S26 in the Supporting Information).

The final step of the catalytic cycle involves the release of the hydroaminated enamine product upon the reaction of **E** with the solvent MeCN proceeding via a transition state TS5 and yielding the solvent-coordinated initiating species **A**. The barrier height for this step to occur is found to be 16.7 kcal/mol from the species **E**, but the large energetic gain in the formation of **E** leads to the barrierless condition from the reactant **A**. The transition state TS5 shows the release of the enamine product [d(Au···C7) = 2.540 Å and d(Au···C6) = 3.144 Å] with subsequent approach of a MeCN solvent molecule [d(Au···N4) = 2.280 Å] (see Figure S18 and Table S21 in the Supporting Information). The imaginary frequency for the transition state TS5 was estimated to be i86 cm^{-1}, showing displacement vectors in the direction of bond formation between the gold and N4 atoms of the MeCN moiety alongside bond dissociation between the gold atom and C6 and C7 atoms of the enamine PhNHMeC═CH_2 moiety.

CONCLUSIONS

In summary, an alkyne and an amine coordination pathway for the hydroamination reaction as catalyzed by a gold(I) (NHC)AuCl-type precatalyst, namely, [1,3-dimethylimidazol-2-ylidene]gold chloride, for the two representative substrates, MeC≡CH and $PhNH_2$, has been modeled using the DFT study. The main conclusions from this work are summarized as follows:

1 The electronic structure of species **A** has been explored in detail using MO and NBO analysis, thus providing useful information on the bonding aspects of this species and how the bonding scenario varies as the reaction progresses. Of particular interest is the gold−carbene carbon (Au−C1) bond length because it offers insight into the nature of the NHC−metal interaction during the course of the catalytic cycle.
2 The mechanistic possibilities explored involve the reaction starting at a common species **A** and then bifurcating into two different pathways, namely, the amine and alkyne coordination ones, leading to another common intermediate **C** with coordinated alkyne and amine ligands. Our energetics reveal that the amine coordination is more favorable by 7 kcal/mol over alkyne coordination, and this electronic preference for this pathway stems from the strong π-acidic nature of alkyne compared to amine.
3 The regiochemistry of the hydroamination product is determined after the formation of an alkyne and amine coordinated intermediate **C**. The intermediate **C** is common to both pathways, after which the reaction proceeds from **C**.
4 From the intermediate **C** onward to regeneration of the catalyst, the catalytic cycle proceeds by an attack of amine on the alkyne, followed by hydrogen migration, which may be an adventitious H_2O- or $PhNH_2$-assisted relay process, finally leading to dissociation of the final product.
5 The role of explicit solvation on hydrogen migration and the fact that the adventitious H_2O or unreacted $PhNH_2$ substrate may reduce the barrier significantly have been explored.
6 Quite interestingly, while regeneration of the catalyst is found to be endothermic, the overall catalytic transformation was found to be thermodynamically favorable by −24.9 kcal/mol, thereby revealing a facile catalytic cycle. The forthcoming catalytic cycles are expected to be even faster because of exothermic stabilization of the end product. The released enamine product PhNHMeC═CH_2 may exist in a tautomeric equilibrium with the relatively more stable imine form PhN═CMe_2 by 7.5 kcal/mol (see Figures S28 and S33−S36 and Tables S22−S25 in the Supporting Information).

EXPERIMENTAL SECTION

General Procedures. All manipulations were carried out using standard Schlenk techniques. Solvents were purified and degassed by standard procedures. [1-(*N*-*tert*-Butylacetamido)-4-benzyl-1,2,4-triazol-5-ylidene]gold chloride was synthesized according to modified literature procedures.[11] Gas chromatography (GC) spectra were obtained on a PerkinElmer Clarus 600 equipped with a flame ionization detector. GC−mass spectrometry (MS) spectra were obtained on a PerkinElmer Clarus 600 T equipped with electron impact source.

Computational Methods. DFT calculations were performed on reactant, product, transition states, and intermediates using the *GAUSSIAN 03*[30] suite of quantum chemical programs. In particular, DFT calculations were performed on the reactant and product species **A**, **B**, **B′**, **C**, **D**, **D′**, and **E** and the transition states TS1 (**A** → **B**), TS1′ (**A** → **B′**), TS2 (**B** → **C**), TS2′ (**B′** → **C**), TS3 (**C** → **D**), TS4 (**D** → **E**) with and without H_2O proton relay, TS4′ (**D** → **D′**), TS4″ (**D′** → **E**), and TS5 (**E** → **A**). The Becke three-parameter exchange functional in conjunction with Lee−Yang−Parr correlation functional (B3LYP) has been employed in the study.[31] The polarized basic set 6-31G(d)[32] was used to describe carbon, nitrogen, and hydrogen atoms. The Stuttgart−Dresden effective core potential (ECP) along with valence basis sets (SDD) was used for the gold atom.[33] Finally, higher-level

dx.doi.org/10.1021/ic2024605 | *Inorg. Chem.* 2012, 51, 5593−5604

single-point calculations were performed on the B3LYP/SDD, 6-31G(d)-optimized geometries using the SDD basis set for the gold atom and the TZVP basis set for all other atoms.[34,35] The relativistic effect of gold has been incorporated by employing the relativistic ECP basis set because accurate all-electron relativistic calculations are extremely time-consuming. These basis sets are routinely used in gold chemistry, and reliable agreement to the experiment has been noted at many occasions.[36]

The transition state optimization method based on the Berny algorithm was used for transition state optimizations.[37] Frequency calculations were performed for all of the optimized structures to characterize the stationary points as minima or the transition states as maxima. The synchronous transit-guided quasi-Newton method developed by Schlegel and co-workers[38] was used to optimize one of the transition states, namely, TS4. The transition states were then additionally confirmed by intrinsic reaction coordinate calculations. Solvation energy has been incorporated using PCM[39] with acetonitrile solvent via a single-point energy computation on the optimized gas-phase geometries. The reported free energies are obtained by correcting the solvation electronic energy with the free-energy correction obtained from the gas-phase structure. All of the energetics of the potential energy surface discussed are thus the solvation free energy unless otherwise stated.

The metal−ligand donor−acceptor interactions were inspected by using CDA[40] at the B3LYP/SDD, 6-31G(d) level of theory, which represents a valuable tool for analyzing the interactions between molecular fragments on a quantitative basis, with an emphasis on electron donation.[41] The donor−acceptor interactions in the various intermediates **A**−**E** of the proposed catalytic cycle were examined using this technique. The orbital interaction between donor and acceptor fragments in **A** {MeCN (donor) and $[(NHC)Au]^+$ (acceptor)}, **B** {[MeC≡CH and MeCN] (donor) and $[(NHC)Au]^+$ (acceptor)}, **B′** {[$PhNH_2$ and MeCN] (donor) and $[(NHC)Au]^+$ (acceptor)}, **C** {[MeC≡CH and $PhNH_2$] (donor) and $[(NHC)Au]^+$ (acceptor)}, **D** {$PhNH_2MeC{=}CH$ moiety (donor) and $[(NHC)Au]^+$ (acceptor)}, **D′** {[PhNHMeC=CH moiety and $(PhNH_3)$] (donor) and $[(NHC)Au]^+$ (acceptor)}, and **E** {$PhNHMeC{=}CH_2$ (donor) and $[(NHC)Au]^+$ (acceptor)}, can be divided into three parts: (i) σ donation from the donor → acceptor fragment (d), (ii) π back-donation from the donor ←acceptor fragment (b), and (iii) a repulsive interaction (r) between the occupied MOs of these two fragments.

The CDA calculations were performed using the *AOMix*[42] program with the B3LYP/SDD, 6-31G(d) wave function. MO compositions and the overlap populations were calculated using the *AOMix* program. Analysis of the MO compositions in terms of occupied and unoccupied fragment orbitals, construction of orbital interaction diagrams, and CDA were performed using the *AOMix-CDA* program.[43]

General Procedure for Hydroamination of Alkynes (under Dry Conditions in the Absence of H_2O). In a typical run, a 25-mL round-bottomed flask was charged with a mixture of [1-(*N*-*tert*-butylacetamido)-4-benzyl-1,2,4-triazol-5-ylidene]gold chloride (2 mol %, 0.01 mmol), $AgBF_4$ (2 mol %, 0.01 mmol), and acetonitrile (ca. 5 mL). To this was added a mixture of 2,6-diethylaniline, phenylacetylene, and diethyleneglycol−di-*n*-butyl ether (internal standard) in a molar ratio of 1:1.5:1. The reaction mixture was heated at 90 °C for 12 h under a nitrogen atmosphere. The reaction was monitored by GC using diethyleneglycol−di-*n*-butyl ether as an internal standard at different time intervals (1, 3, 7, and 12 h; see Figure S27 in the Supporting Information).

General Procedure for Hydroamination of Alkynes (in the Presence of Varying Amounts of H_2O). In a typical run, a 25-mL round-bottomed flask was charged with a mixture of [1-(*N*-*tert*-butylacetamido)-4-benzyl-1,2,4-triazol-5-ylidene]gold chloride (2 mol %, 0.01 mmol), $AgBF_4$ (2 mol %, 0.01 mmol), and acetonitrile (ca. 5 mL). To this was added a mixture of 2,6-diethylaniline, phenylacetylene, and diethyleneglycol−di-*n*-butyl ether (internal standard) in a molar ratio of 1:1.5:1. Depending upon the specific experiment, varying amounts of H_2O (1, 10, or 100 μL) were added. The reaction mixture was heated at 90 °C for 12 h under a nitrogen atmosphere. The reaction was monitored by GC using diethyleneglycol−di-*n*-butyl ether as an internal standard at different time intervals (1, 3, 7, and 12 h; see Figure S27 in the Supporting Information).

General Procedure of the Blank Experiment. In a typical run, a 25-mL round-bottomed flask was charged with $AgBF_4$ (2 mol %, 0.01 mmol) and acetonitrile (ca. 5 mL). To this was added a mixture of 2,6-diethylaniline, phenylacetylene, and diethyleneglycol−di-*n*-butyl ether (internal standard) in a molar ratio of 1:1.5:1. The reaction mixture was heated at 90 °C for 12 h under a nitrogen atmosphere. The reaction was monitored by GC using diethyleneglycol−di-*n*-butyl ether as an internal standard at different time intervals (1, 3, 7, and 12 h; see Figure S27 in the Supporting Information).

■ ASSOCIATED CONTENT

Ⓢ Supporting Information

Complete ref 30 and the molecular geometries and electronic energies of all species. This material is available free of charge via the Internet at http://pubs.acs.org.

■ AUTHOR INFORMATION

Corresponding Author

*E-mail: pghosh@chem.iitb.ac.in (P.G.), rajaraman@chem.iitb.ac.in (G.R.), Fax: +91-22-2572-3480.

Notes

The authors declare no competing financial interest.

■ ACKNOWLEDGMENTS

We thank Board of Research in Nuclear Sciences, Mumbai, India, for financial support of this research. Computational facilities from the Indian Institute of Technology Bombay Computer Center are gratefully acknowledged.

■ REFERENCES

(1) (a) Hashmi, A. S. K.; Buhrle, M. *Aldrichim. Acta* **2010**, *43*, 27−33. (b) Francisco, A.; Irina, P. B.; Miguel, Y. *Chem. Rev.* **2004**, *104*, 3079−3159. (c) Yoshinori, Y.; Ukkiramapandian, R. *Chem. Soc. Rev.* **1999**, *28*, 199−207.

(2) For recent examples, see: (a) Hansen, M. C.; Heusser, C. A.; Narayan, T. C.; Fong, K. E.; Hara, N.; Kohn, A. W.; Venning, A. R.; Rheingold, A. L.; Johnson, A. R. *Organometallics* **2011**, *30*, 4616−4623. (b) Liu, L.; Wang, F.; Wang, W.; Zhao, M.; Shi, M. *Beilstein J. Org. Chem.* **2011**, *7*, 555−564. (c) Ayinla, R. O.; Schafer, L. L. *Dalton Trans.* **2011**, *40*, 7769−7776. (d) Wixey, J. S.; Ward, B. D. *Dalton Trans.* **2011**, *40*, 7693−7696. (e) Yadav, J. S.; Antony, A.; Rao, T. S.; Reddy, B. V. S. *J. Organomet. Chem.* **2011**, *696*, 16−36. (f) Specht, Z. G.; Cortes-Llamas, S. A.; Tran, H. N.; Niekerk, C. J. V.; Rancudo, K. T.; Golen, J. A.; Moore, C. E.; Rheingold, A. L.; Dwyer, T. J.; Grotjahn, D. B. *Chem.—Eur. J.* **2011**, *17*, 6606−6609. (g) Dash, C.; Shaikh, M. M.; Butcher, R. J.; Ghosh, P. *Dalton Trans.* **2010**, *39*, 2515−2524. (h) Broderick, E. M.; Gutzwiller, N. P.; Diaconescu, P. L. *Organometallics* **2010**, *29*, 3242−3251. (i) Hashmi, A. S. K.; Rudolph, M.; Schymura, S.; Visus, J.; Frey, W. *Eur. J. Org. Chem.* **2006**, 4905−4909.

(3) (a) Kinjo, R.; Donnadieu, B.; Bertrand, G. *Angew. Chem., Int. Ed.* **2011**, *50*, 5560−5563. (b) Luhl, A.; Nayek, H. P.; Blechert, S.; Roesky, P. W. *Chem. Commun.* **2011**, *47*, 8280−8282. (c) Yuan, D.; Tang, H.; Xiao, L.; Huynh, H. V. *Dalton Trans.* **2011**, *40*, 8788−8795. (d) Ito, H.; Harada, T.; Ohmiya, H.; Sawamura, M. *Beilstein J. Org. Chem.* **2011**, *7*, 951−959. (e) Sarma, R.; Prajapati., D. *Chem. Commun.* **2011**, *47*, 9525−9527. (f) Arndt, M.; Salih, K. S. M.; Fromm, A.; Goossen, L. J.; Menges, F.; Niedner-Schatteburg, G. *J. Am. Chem. Soc.* **2011**, *133*, 7428−7449. (g) Patil, N. T.; Singh, V. *J. Organomet. Chem.* **2011**, *696*, 419−432. (h) Reyes-Sanchez, A.; Canavera-Buelvas, F.; Barrios-Francisco, R.; Cifuentes-Vaca, O. L.; Flores-Alamo, M.; García, J. J. *Organometallics* **2011**, *30*, 3340−3345. (i) Tokimizu, Y.; Ohta, Y.; Chiba, H.; Oishi, S.; Fujii, N.; Ohno, H. *Tetrahedron* **2011**, *67*, 5168−5175. (j) Kumaran, E.; Sridevi, V. S.; Leong, W. K. *Organometallics*

2010, *29*, 6417−6421. (k) Leyva-Perez, A.; Cabrero-Antonino, J. R.; Cantin, A.; Corma, A. *J. Org. Chem.* **2010**, *75*, 7769−7780. (l) Patil, N. T.; Lakshmi, P. G. V. V.; Singh, V. *Eur. J. Org. Chem.* **2010**, 4719−4731. (m) Patil, N. T.; Singh, V.; Konala, A.; Mutyala, A. K. *Tetrahedron Lett.* **2010**, *51*, 1493−1496. (n) Deju, Y.; Wang, J.; Zhang, X.; Zhou, Y.; Ding, X.; Feng, E.; Sun, H.; Liu, G.; Jiang, H.; Liu, H. *Green Chem.* **2009**, *11*, 1201−1208. (o) Pasha, N.; Babu, N. S.; Rao, K. T. V.; Prasad, P. S.; Lingaiah, N. *Tetrahedron Lett.* **2009**, *50*, 239−242. (p) Lai, R.; Surekha, K.; Hayashi, A.; Ozawa, F.; Liu, Y.; Peng, S.; Liu, S. *Organometallics* **2007**, *26*, 1062−1068. (q) Takaki, K.; Koizumi, S.; Yamamoto, Y.; Komeyama, K. *Tetrahedron Lett.* **2006**, *47*, 7335−7337. (r) Burling, S.; Field, L. D.; Messerle, B. A. *Organometallics* **2000**, *19*, 87−90.

(4) (a) Thomas, E. M.; Kai, C. H.; Miguel, Y.; Francisco, F.; Mizuki, T. *Chem. Rev.* **2008**, *108*, 3795−3892. (b) Thomas, E. M.; Matthias, B. *Chem. Rev.* **1998**, *98*, 675−703.

(5) (a) Rene, S.; Sven, D. *Chem. Soc. Rev.* **2007**, *36*, 1407−1420. (b) Frauke, P.; Sven, D. *Chem. Soc. Rev.* **2003**, *32*, 104−114.

(6) Straub, T.; Haskel, A.; Neyroud, T. G.; Kapon, M.; Botoshansky, M.; Eisen, M. S. *Organometallics* **2001**, *20*, 5017−5035.

(7) Mizushima, E.; Hayashi, T.; Tanaka, M. *Org. Lett.* **2003**, *5*, 3349−3352.

(8) Larock, R. C. *Angew. Chem., Int. Ed. Engl.* **1978**, *17*, 27−37.

(9) (a) Dion, I.; Beauchemin, A. M. *Angew. Chem., Int. Ed.* **2011**, *50*, 8233−8235. (b) Shapiro, N. D.; Rauniyar, V.; Hamilton, G. L.; Wu, J.; Toste, F. D. *Nat. Chem.* **2011**, *470*, 245−250. (c) Terada, M. *Synthesis* **2010**, *12*, 1929−1982. (d) Akiyama, T. *Chem. Rev.* **2007**, *107*, 5744−5758.

(10) (a) Tamer, A.; Moris, S. E. *Chem. Soc. Rev.* **2008**, *37*, 550−567. (b) Gary, A.; Antoinette, C. R. *Chem. Rev.* **2002**, *102*, 2161−2185.

(11) Dash, C.; Shaikh, M. M.; Butcher, R. J.; Ghosh, P. *Inorg. Chem.* **2010**, *49*, 4972−4983.

(12) John, A.; Ghosh, P. *Dalton Trans.* **2010**, *39*, 7183−7206.

(13) (a) Ray, L.; Katiyar, V.; Barman, S.; Raihan, M. J.; Nanavati, H.; Shaikh, M. M.; Ghosh, P. *J. Organomet. Chem.* **2007**, *692*, 4259−4269. (b) Samantaray, M. K.; Katiyar, V.; Pang, K.; Nanavati, H.; Ghosh, P. *J. Organomet. Chem.* **2007**, *692*, 1672−1682. (c) Ray, L.; Katiyar, V.; Raihan, M.; Nanavati, H.; Shaikh, M. M.; Ghosh, P. *Eur. J. Inorg. Chem.* **2006**, 3724−3730. (d) Samantaray, M. K.; Roy, D.; Patra, A.; Stephen, R.; Saikh, M.; Sunoj, R. B.; Ghosh, P. *J. Organomet. Chem.* **2006**, *691*, 3797−3805. (e) Samantaray, M. K.; Katiyar, V.; Roy, D.; Pang, K.; Nanavati, H.; Stephen, R.; Sunoj, R. B.; Ghosh, P. *Eur. J. Inorg. Chem.* **2006**, 2975−2984.

(14) (a) Kumar, S.; Shaikh, M. M.; Ghosh, P. *J. Organomet. Chem.* **2009**, *694*, 4162−4169. (b) Ray, L.; Shaikh, M. M.; Ghosh, P. *Dalton Trans.* **2007**, 4546−4555. (c) Ray, L.; Shaikh, M. M.; Ghosh, P. *Organometallics* **2007**, *26*, 958−964.

(15) (a) Samantaray, M. K.; Shaikh, M. M.; Ghosh, P. *J. Organomet. Chem.* **2009**, *694*, 3477−3486. (b) John, A.; Shaikh., M. M.; Ghosh, P. *Dalton Trans.* **2009**, 10581−10591. (c) Dash, C.; Shaikh, M. M.; Ghosh, P. *Eur. J. Inorg. Chem.* **2009**, 1608−1618. (d) Ray, L.; Barman, S.; Shaikh, M. M.; Ghosh, P. *Chem.—Eur. J.* **2008**, *14*, 6646−6655.

(16) (a) Kumar, S.; Narayanan, A.; Rao, M. N.; Shaikh, M. M.; Ghosh, P. *J. Organomet. Chem.* **2012**, *696*, 4159−4165. (b) Samantaray, M. K.; Shaikh, M. M.; Ghosh, P. *Organometallics* **2009**, *28*, 2267−2275. (c) Ray, S.; Shaikh., M. M.; Ghosh, P. *Eur. J. Inorg. Chem.* **2009**, 1932−1941.

(17) Dash, C.; Shaikh, M. M.; Butcher, R. J.; Ghosh, P. *Dalton Trans.* **2010**, *39*, 2515−2524.

(18) Stephen, R.; Sunoj, R. B.; Ghosh, P. *Dalton Trans.* **2011**, *40*, 10156−10161.

(19) (a) Leitch, D. C.; Platel, R. H.; Schafer, L. L. *J. Am. Chem. Soc.* **2011**, *133*, 15453−15463. (b) Arndt, M.; Salih, K. S. M.; Fromm, A.; Goossen, L. J.; Menges, F.; Niedner-Schatteburg, G. *J. Am. Chem. Soc.* **2011**, *133*, 7428−7449. (c) Beauchemin, A. M.; Moran, J.; Lebrun, M.; Dimitrijevic, C. S.; Zhang, L.; Gorelsky, S. I. *Angew. Chem., Int. Ed.* **2008**, *47*, 1410−1413. (d) Straub, B. F.; Bergman, R. G. *Angew. Chem., Int. Ed.* **2001**, *40*, 4632−4635.

(20) (a) Fukuda, Y.; Utimoto, K. *J. Org. Chem.* **1991**, *56*, 3729−3731. (b) Fukuda, Y.; Utimoto, K. *Synthesis* **1991**, 975−978. (c) Fukuda, Y.; Utimoto, K.; Nozaki, H. *Heterocycles* **1987**, *25*, 297−300.

(21) Kovacs, G.; Lledos, A.; Ujaque, G. *Angew. Chem., Int. Ed.* **2011**, *50*, 11147−11151.

(22) (a) Lein, M.; Rudolph, M.; Hashmi, A. S. K.; Schwerdtfeger, P. *Organometallics* **2010**, *29*, 2206−2210. (b) Pernpointner, M.; Hashmi, A. S. K. *J. Chem. Theory Comput.* **2009**, *5*, 2717−2725.

(23) Krauter, C. M.; Hashmi, A. S. K.; Pernpointner, M. *ChemCatChem* **2010**, *2*, 1226−1230.

(24) Comas-Vives, A.; Harvey, J. N. *Eur. J. Inorg. Chem.* **2011**, 5025−5035.

(25) Cotton, F. A.; Wilkinson, G.; Murillo, C. A.; Bochmann, M. *Advanced Inorganic Chemistry*, 6th ed.; John Wiley & Sons, Inc.: New York, 1999; pp 1084−1107.

(26) Pauling, L. *The Nature of the Chemical Bond*, 3rd ed.; Cornell University Press: Ithaca, NY, 1960; pp 224−228, 256−257.

(27) (a) Benitez, D.; Shapiro, N. D.; Tkatchouk, E.; Wang, Y.; Goddard, W. A.; Toste, F. D. *Nat. Chem.* **2009**, *1*, 482−486. (b) Nemcsok, D.; Wichmann, K.; Frenking, G. *Organometallics* **2004**, *23*, 3640−3646. (c) Boehme, C.; Frenking, G. *Organometallics* **1998**, *17*, 5801−5809.

(28) Zeng, X.; Soleilhavoup, M.; Bertrand, G. *Org. Lett.* **2009**, *11*, 3166−3169.

(29) (a) Anand, M.; Sunoj, R. B. *Org. Lett.* **2011**, *13*, 4802−4805. (b) Patil, M. P.; Sunoj, R. B. *Chem.—Eur. J.* **2008**, *14*, 10472−10485. (c) Roy, D.; Sunoj, R. B. *Chem.—Eur. J.* **2008**, *14*, 10530−10534.

(30) Frisch, M. J. et al. *GAUSSIAN 03*, revision C.02; Gaussian, Inc.: Wallingford, CT, 2004.

(31) (a) Becke, A. D. *Phys. Rev. A* **1988**, *38*, 3098−3100. (b) Lee, C.; Yang, W.; Parr, R. G. *Phys. Rev. B* **1988**, *37*, 785−789.

(32) (a) Hehre, W. J.; Ditchfield, R.; Pople, J. A. *J. Chem. Phys.* **1972**, *56*, 2257−2261. (b) Petersson, G. A.; Bennet, A.; Tensfeldt, T. G.; Al-Laham, M. A.; Shirley, W. A.; Mantzaris, J. *J. Chem. Phys.* **1988**, *89*, 2193−2218. (c) Petersson, G. A.; Al-Laham, M. A. *J. Chem. Phys.* **1991**, *94*, 6081−6090.

(33) (a) Faza, O. N.; Lopez, C. S.; Alvarez, R.; de Lera, A. R. *J. Am. Chem. Soc.* **2006**, *128*, 2434−2437. (b) Wang, X.; Andrews, L. *J. Am. Chem. Soc.* **2001**, *123*, 12899−12900.

(34) (a) Weigenda, F.; Ahlrichs, R. *Phys. Chem. Chem. Phys.* **2005**, *7*, 3297−3305. (b) Schafer, A.; Horn, H.; Ahlrichs, R. *J. Chem. Phys.* **1992**, *97*, 2571−2577.

(35) (a) Li, Z.; Zhao, Y.; Wu, X.; Ding, X.; He, S. *Chem.—Eur. J.* **2011**, *17*, 11728−11733. (b) Kiran, R. V.; Hogan, C. F.; James, B. D.; Wilson, D. J. D. *Eur. J. Inorg. Chem.* **2011**, 4816−4825. (c) Xu, X.; Truhlar, D. G. *J. Chem. Theory Comput.* **2011**, *7*, 2766−2779. (d) Gutmann, T.; Walaszek, B.; Yeping, Y.; Wachtler, M.; Rosal, I.; Grunberg, A.; Poteau, R.; Axet, R.; Lavigne, G.; Chaudret, B.; Limbach, H.; Buntkowsky, G. *J. Am. Chem. Soc.* **2010**, *132*, 11759−11767. (e) Sauriol, F.; Sonnenberg, J. F.; Chadder, S. J.; Dunlop-Briere, A. F.; Baird, M. C.; Budzelaar, P. H. M. *J. Am. Chem. Soc.* **2010**, *132*, 13357−13370.

(36) (a) Pyykko, P.; Stanton, J. F. *Chem. Rev.* **2012**, *112*, 1−3. (b) Pyykko, P. *Chem. Soc. Rev.* **2008**, *37*, 1967−1997. (c) Pyykko, P. *Inorg. Chim. Acta* **2005**, *358*, 4113−4130. (d) Schroder, D.; Hrusak, J.; Tornieporth-Oetting, I.; Klapotke, T. M.; Schwarz, H. *Angew. Chem., Int. Ed. Engl.* **1994**, *33*, 212−214. (e) Pyykko, P. *Chem. Rev.* **1988**, *88*, 563−594.

(37) (a) Gonzalez, C.; Schlegel, H. B. *J. Chem. Phys.* **1989**, *90*, 2154−2161. (b) Schlegel, H. B. In *New Theoretical Concepts for Undergraduating Organic Reaction*; Bertran, J., Ed.; Kluwer Academic: Amsterdam, The Netherlands, 1989; pp 33−53.

(38) (a) Peng, C.; Ayala, P. Y.; Schlegel, H. B.; Frisch, M. J. *J. Comput. Chem.* **1996**, *17*, 49−56. (b) Peng, C.; Schlegel, H. B. *Isr. J. Chem.* **1994**, *33*, 449−454.

(39) (a) Cossi, M.; Scalmani, G.; Rega, N.; Barone, V. *J. Chem. Phys.* **2002**, *117*, 43−54. (b) Cossi, M.; Barone, V.; Cammi, R.; Tamasi, J. *Chem. Phys. Lett.* **1996**, *255*, 327−335. (c) Miertus, S.; Scrocco, E.; Tamasi, J. *Chem. Phys.* **1981**, *55*, 117−129.

(40) Dapprich, S.; Frenking, G. *J. Phys. Chem.* **1995**, *99*, 9352−9362.
(41) Vyboishchikov, S. F.; Frenking, G. *Chem.—Eur. J.* **1998**, *4*, 1439−1448.
(42) Gorelsky, S. I.; Lever, A. B. P. *J. Organomet. Chem.* **2001**, *635*, 187−196.
(43) Gorelsky, S. I.; Ghosh, S.; Solomon, E. I. *J. Am. Chem. Soc.* **2006**, *128*, 278−290.